

· 基础研究 ·

大鼠牙齿空间移动评估及牙槽骨微观结构变化追踪研究

钱心瑶^{1,2,3,4}, 姜迪⁵, 谢玉婷^{2,3,4}, 吴斌⁵, 唐雯^{1,2,3,4}, 陆玲波^{1,2,3,4}, 李禹江⁵, 谢理哲^{2,4*}, 严斌^{1,2,3,4*}

¹南京医科大学附属口腔医院正畸科, 江苏 南京 210029; ²口腔疾病研究与防治国家级重点实验室培育建设点, 江苏 南京 210029; ³江苏省口腔转化医学工程研究中心, 江苏 南京 210029; ⁴南京医科大学口腔数字化医疗技术工程中心, 江苏 南京 210029; ⁵南京林业大学机械电子工程学院, 江苏 南京 210037

[摘要] 目的: 显微CT(micro-computed tomography, Micro-CT)活体扫描观测并量化正畸力下大鼠的牙齿移动, 张力区及压力区骨小梁微观结构的连续变化情况。方法: 对5只雄性8周龄SD大鼠的左侧上颌第一磨牙施加50 g矫治力, 使用Micro-CT在加力前及加力后的不同时间点对大鼠进行活体扫描, 在统一空间坐标系下计算大鼠正畸牙齿移动距离, 并测量统计移动牙张力区及压力区的骨小梁微观形态和力学特性相关参数, 分析其动态变化特征。结果: 大鼠磨牙在0~3 d有明显位移, 3~14 d移动速率下降, 21~28 d速率增加($P < 0.001$); 张力区及压力区多项骨小梁参数分别以7、14 d为转折点, 骨体积分数(bone volume fraction, BV/TV)和骨小梁厚度(trabecular thickness, Tb.Th)先下降后升高, 孔隙总体积[total volume of pore space, Po.V(tot)], 结构模型指数(structure model index, SMI)、骨小梁间隙(trabecular separation, Tb.Sp)和分形维数(fractal dimension, FD)先升高后下降, 牙移动前期张力区增量斜率较压力区更大, 牙移动后期BV/TV、Po.V(tot)、SMI和Tb.Sp数值在张力区及压力区差异有统计学意义(P 均 < 0.05)。结论: 大鼠正畸牙移动具有三阶段性; 张力区及压力区骨小梁微观结构改建存在差异, 骨量及骨质量均先降低后升高, 并分别在7 d和14 d前后达到最低点; 张力区的骨吸收活跃期较早, 张力区牙槽骨骨形成滞后于压力区骨吸收。

[关键词] Micro-CT; 正畸牙齿移动; 骨小梁; 微观结构; 追踪研究**[中图分类号]** R783.5**[文献标志码]** A**[文章编号]** 1007-4368(2025)04-478-10**doi:** 10.7655/NYDXBNSN241230

Evaluation of tooth spatial movement and tracking of microstructural changes in the alveolar bone in rats

QIAN Xinyao^{1,2,3,4}, JIANG Di⁵, XIE Yuting^{2,3,4}, WU Bin⁵, TANG Wen^{1,2,3,4}, LU Lingbo^{1,2,3,4}, LI Yujiang⁵, XIE Lizhe^{2,4*}, YAN Bin^{1,2,3,4*}¹Department of Orthodontics, the Affiliated Stomatological Hospital of Nanjing Medical University, Nanjing 210029;²State Key Laboratory Cultivation Base of Research, Prevention and Treatment for Oral Diseases, Nanjing 210029;³Jiangsu Province Engineering Research Center of Stomatological Translational Medicine, Nanjing 210029; ⁴Oral Digital Medical Technology Engineering Center, Nanjing Medical University, Nanjing 210029; ⁵College of Mechanical and Electronic Engineering, Nanjing Forestry University, Nanjing 210037, China

[Abstract] **Objective:** This study was aimed to observe and quantify the continuous changes in dental movement and trabecular microstructure in both tension and pressure zones of rats under orthodontic force using the *in vivo* micro-computed tomography (Micro-CT) scanning. **Methods:** A 50 g orthodontic force was applied to the left maxillary first molar of five 8-week-old male SD rats. The rats were scanned *in vivo* at different time points using Micro-CT. The distance of orthodontic tooth movement was calculated in a unified spatial coordinate system. Additionally, trabecular micro-morphological and mechanical property-related parameters in the tension and

[基金项目] 国家自然科学基金(82371000, 82071143, 82101079); 国家重点研发计划(2022YFC2402103, 2023YFC2413605); 江苏省重点研发计划(BE2022795); 江苏省科学技术厅社会发展面上项目(BE2023836)

*通信作者(Corresponding author), E-mail: xielizhe@njmu.edu.cn (ORCID: 0000-0001-7763-9492); byan@njmu.edu.cn (ORCID: 0000-0001-9169-4615)

pressure zones of the moving teeth were measured and statistically analyzed. **Results:** There was significant displacement of the rat molars within the first 0–3 days, with a decrease in movement rate between 3 and 14 days, followed by an increase in rate between 21 and 28 days ($P < 0.001$). Multiple trabecular parameters in both tension and pressure zones showed turning points at 7 days and 14 days, respectively. Specifically, the values of bone volume fraction (BV/TV) and trabecular thickness (Tb.Th) were first decreased and then increased, while those of total porosity volume [Po.V (tot)], structure model index (SMI), trabecular separation (Tb.Sp), and fractal dimension (FD) exhibited the opposite trend. During the early stage of tooth movement, the slope of increase in trabecular parameters was greater in the tension zone compared with the pressure zone. In the later stage of tooth movement, there were significant differences in the values of BV/TV, Po.V (tot), SMI, and Tb.Sp between the tension and pressure zones (P all < 0.05). **Conclusion:** Orthodontic tooth movement in rats occurs in three stages. There are differences in trabecular microstructure remodeling between tension and pressure zones, with bone mass and bone quality both decreasing first and then increasing, reaching their lowest points around 7 days and 14 days, respectively. The active phase of bone resorption in the tension zone occurs early, and bone formation in the alveolar bone of the tension zone lags behind bone resorption in the pressure zone.

[Key words] Micro-CT; orthodontic tooth movement; trabecular bone; micro-structure; longitudinal study

[J Nanjing Med Univ, 2025, 45(04): 478-486, 522]

正畸牙移动(orthodontic tooth movement, OTM)是牙周组织在机械力作用下发生骨重塑的结果^[1],压力侧表现为破骨细胞介导的骨吸收,而张力侧为成骨细胞介导的骨形成^[2]。外部载荷会影响骨密度和骨小梁三维结构^[3-4],进而影响骨强度^[5]。

以往研究主要关注 OTM 期间的骨量或密度变化^[6-7],且局限于组织学切片、扫描电子显微镜等二维观测^[6,8],少有研究聚焦于松质骨多孔介质,特别是骨小梁微观形态结构的三维变化。尽管有学者通过动物实验研究牙槽骨变化,但通常为静态观察^[9-12],即在特定时间点处死动物后进行离体扫描,且多关注大鼠第一磨牙的根分叉区域^[9-11]以及某一牙根的受压侧^[12-13]。有研究报道加力2周后压力侧骨小梁更加致密^[14],张力侧骨质在0~14 d内逐渐疏松^[15],另有研究指出正畸力下压力区骨密度迅速降低,但0、3、7 d时张力区骨量无显著变化^[16]。这些离体观测实验无法准确评估特定参数的动态变化,因此有关骨小梁改建特性、趋势以及不同受力区差异的结论仍存在争议。此外,现有研究常将大鼠磨牙的近中倾斜移动简化为平动处理^[17],导致测量结果难以真实反映牙齿移动情况。松质骨具有不均一性和各向异性等力学特征^[18],但当前常见的骨小梁形态评价指标较为局限,缺乏对多孔介质力学属性的评估。因此,亟需提出新的实验思路,以有效量化正畸力下牙齿移动和不同受力区骨小梁微观结构的改建情况,为后续生物学研究提供坚实基础。

显微CT(micro-computed tomography, Micro-CT)作为一种新型高分辨率CT影像检测与分析技术,能对骨的微观结构特性进行三维成像分析^[19]。对于

小型动物,还可通过活体扫描对牙移动和骨改建过程进行动态纵向研究,克服以往研究的局限性。因此,本研究利用 Micro-CT 进行个体追踪,在不同时间点进行活体扫描,建立统一空间坐标系测量真实牙移动距离,引入与力学属性相关的形态学参数,持续监测张力区及压力区骨小梁显微结构变化,并探究两区域的差异与特征,旨在为正畸力下牙槽骨微结构改建趋势、时间点及力学性能变化提供新见解,为临床正畸提供参考。

1 材料和方法

1.1 材料

选取5只健康雄性8周龄SD大鼠,体重(230±25)g,由北京维通利华实验动物技术有限公司供给。实验方案经过南京医科大学伦理委员会审查批准(批准号:IACUC-2205040)。实验前,按0.12 mL/100 g注射3%戊巴比妥钠对大鼠进行腹腔麻醉。选取上颌左侧为加力侧,用0.25 mm结扎丝(杭州西湖巴尔公司)穿过左侧上颌第一磨牙与第二磨牙邻间隙,将镍钛拉簧(上海埃蒙迪公司)固定于第一磨牙和上颌切牙之间,由正畸测力计测得力值约50 g,牵引上颌左侧第一磨牙向近中移动(图1A、B)。上下颌切牙用光固化纳米树脂(3M公司,美国)包裹防止结扎丝脱落及拉簧断裂,持续加力28 d,每日检查加力装置的固位情况,并确认大鼠上颌切牙无明显移位及折裂。

1.2 方法

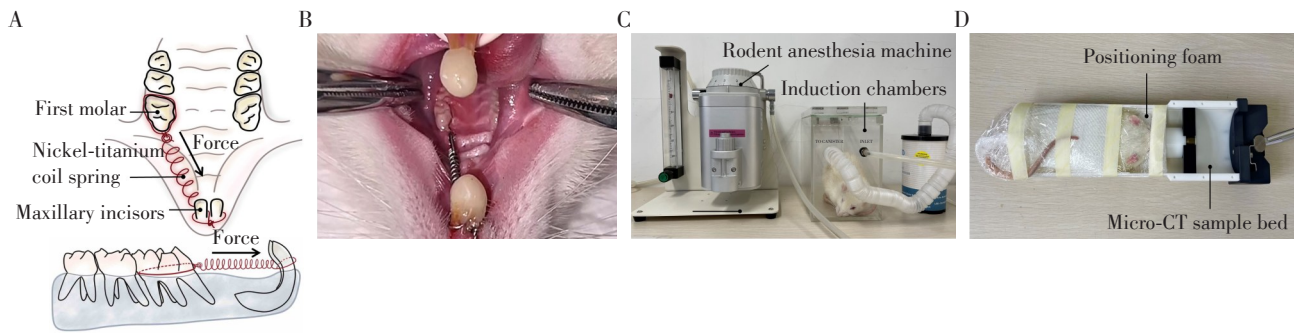
1.2.1 Micro-CT活体扫描

在加力前(0 d)及加力后3、7、14、21、28 d,使用Micro-CT(Skyscan 1173, Bruker公司,德国)对大鼠

进行活体扫描。为避免金属伪影,每次扫描前用异氟烷(3%~4%,5~6 min)吸入法麻醉大鼠(图1C),将口内加力装置拆除。将大鼠腹部朝下放于碳素样品床中,大鼠头部用塑料泡沫装置固定,使其腭平面与台面平行(图1D)。扫描过程中持续输入0.8 L/min氧气及2%异氟烷维持麻醉。Micro-CT扫描条件设置为70 kVp、114 μ A、8 W,扫描精度为17.5 μ m,目标区域为左侧上颌第一、二磨牙及周围牙槽骨,每次扫描时间约40 min。使用NRecon软件(Bruker公司,德国)进一步重建原始数据,每只大鼠每个时间点可生成约660张横截面图像,分辨率为1 395 \times 1 409像素。

1.2.2 OTM距离及骨小梁参数测量

将Micro-CT扫描获得的原始数据以DICOM(digital imaging and communications in medicine)格式导出,在Amira软件(v6.0, Thermo Fisher Scientific公司,美国)中对上颌扫描区域进行三维重建,定位上腭部腭后孔,并以腭后孔前缘点为原点O建立了统一的空间坐标系。该坐标系中, x 轴和 y 轴平行于腭平面, x 轴方向与施力方向一致, z 轴垂直于腭平面。使用与大鼠活体扫描相同的参数设置,扫描Micro-CT配套的标准密度体模(Bruker公司,德国),在Amira软件中测定5个不同密度区域所对应的CT值,并拟合成线性曲线,根据公式(1)将磨牙各区域



A: Schematic diagram of orthodontic tooth movement in rats. B: Intraoral photo of rat teeth after force application. C: Inhalation anesthesia of rats before Micro-CT scanning. D: The rat was immobilized on the sample bed.

图1 大鼠正畸牙移动模型

Figure 1 Orthodontic tooth movement model in rats

的CT值转换为密度值: $HU=2\ 031+10.61\times\rho$ (1),其中, ρ 表示密度值, HU 表示CT值。

将牙齿区域内的所有像素点视为离散的质点,每个质点具有特定的坐标 (x_n, y_n, z_n) 和相应的密度值。这些质点共同构成了1个质点系。通过以下公式(2)、(3)、(4)计算该质点系的质心坐标 $(\bar{x}, \bar{y}, \bar{z})$:

$$\bar{x} = \frac{M_y}{M} = \frac{\sum_{i=1}^n m_i x_i}{\sum_{i=1}^n m_i} = \frac{\sum_{i=1}^n \rho_i V_i x_i}{\sum_{i=1}^n \rho_i V_i} \quad (2)$$

$$\bar{y} = \frac{M_z}{M} = \frac{\sum_{i=1}^n m_i y_i}{\sum_{i=1}^n m_i} = \frac{\sum_{i=1}^n \rho_i V_i y_i}{\sum_{i=1}^n \rho_i V_i} \quad (3)$$

$$\bar{z} = \frac{M_x}{M} = \frac{\sum_{i=1}^n m_i z_i}{\sum_{i=1}^n m_i} = \frac{\sum_{i=1}^n \rho_i V_i z_i}{\sum_{i=1}^n \rho_i V_i} \quad (4)$$

其中, M 表示质点系的总质量, m_i 、 V_i 和 ρ_i 分别表示第*i*个质点的质量、体素和密度。静矩用于描述

质点系在该平面上的分布情况, M_y 、 M_z 和 M_x 分别表示质点系对 yz 、 xz 和 xy 平面的静矩。由上述公式可得第一、第二磨牙质心的空间坐标,以第一磨牙质心为起点、第二磨牙质心为终点的有向线段为向量 \vec{D} ,将该向量平移至坐标系原点,其在 x 轴投影的长度即为牙齿移动量。

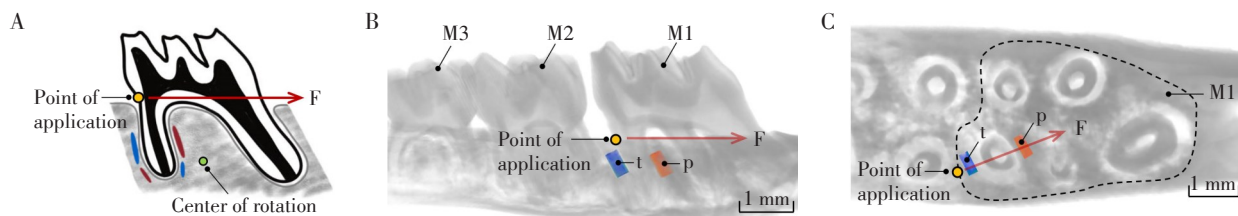
本研究选取左上颌第一磨牙远中颊根中部的近中及远中牙槽松质骨作为感兴趣区(region of interest, ROI),并遵循以下原则:依据加力方向将远中颊根的近中侧作为压力区(ROI-p)、远中侧作为张力区(ROI-t),分别框选1个150 μ m \times 400 μ m \times 400 μ m的长方体(图2),其顶面位于远中颊根根分叉至根尖的上1/3与中1/3交界处。在Amira软件中对所选ROI进行三维重建,从长方体顶面宽度中点处截取纵切面。将DICOM文件依次导入Dataviewer、CTAn软件(Bruker公司,德国)完成校正及切片后,对骨小梁的显微结构进行定量分析。主要测量参数包括骨体积分数(bone volume fraction, BV/TV)、结构模

型指数(structure model index, SMI)、骨小梁厚度(trabecular thickness, Tb.Th)、骨小梁间隙(trabecular separation, Tb.Sp)、骨小梁数目(trabecular number, Tb.N)、孔隙总体积[total volume of pore space, Po.V(tot)]、分形维数(fractal dimension, FD)。为确

保测量结果的可靠性,所有测量值间隔1周后由同一操作者重复测量3次并取平均值。

1.3 统计学方法

使用SPSS 20.0进行统计分析,经Shapiro-Wilk检验,本研究数据均符合正态分布,以均数±标准差



A: Schematic diagram of force application on the first molar in rats, F indicates the direction of force application. The red band represents the pressure zone determined based on the center of rotation, while the blue band indicates the tension zone. B: Sagittal view, ROI-p denotes the pressure zone, and ROI-t denotes the tension zone. The width of the ROI is 150 μm , and the height is 400 μm . M1 represents the first molar, M2 represents the second molar, and M3 represents the third molar(scale bar=1 mm). C: Axial view, the width of the ROI is 150 μm , and the length is 400 μm .

图2 骨小梁参数测量的ROI示意图

Figure 2 Schematic diagram of ROI for trabecular parameter measurement

($\bar{x} \pm s$)表示。通过单因素方差分析和Tukey事后检验比较相邻时间点牙齿移动距离和骨小梁参数的差异,采用独立样本t检验比较张力区与压力区的骨小梁参数及其增量。 $P < 0.05$ 表示差异有统计学意义。

2 结果

2.1 正畸牙齿移动距离

牙齿移动的Micro-CT三维重构图像显示,大鼠左侧上颌第一磨牙在镍钛拉簧的作用下,0~28 d内持续向近中移动(图3A)。Amira软件测定的密度-CT值线性拟合曲线见图3B,质心距离测量法示意图见图3C。牙移动距离变化见图3D,在牙移动初期,0~3 d内OTM速率较大,提示前3 d为快速移动阶段,为初始快速期;随后,3~7 d及7~14 d中OTM速率均减缓,为平台期;14 d后,为快速线性移动期,牙齿移动进入线性阶段,OTM速率迅速增加,21~28 d移动量最大,各时间点差异显著(P 均 < 0.001)。

2.2 牙槽骨骨小梁微观结构变化

2.2.1 ROI三维重建截面图

在Micro-CT矢状位及横断位切片中选取ROI(图4A)。ROI三维重建显示,加力至14 d,大鼠第一磨牙远颊根压力区牙槽骨骨量减少,骨小梁形态被破坏,分离度增大,孔隙增多,14 d最明显且呈非均匀凹陷;之后,各参数变化趋势转变,21、28 d压力区骨量逐渐回升,孔隙缩减,但28 d尚未恢复至初始状态。张力区前7 d内骨小梁结构形态变化与压力区类似,但孔隙数量、宽度的增长较少,14~28 d骨

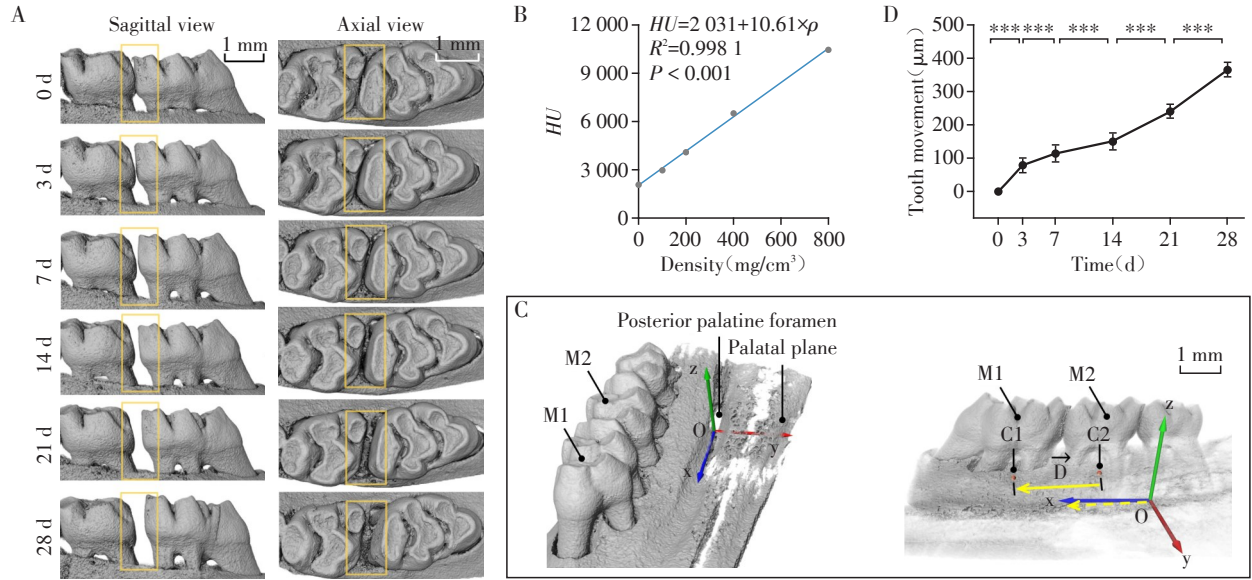
组织占比持续增加(图4B)。

2.2.2 骨小梁三维形态结构变化

14、21、28 d时张力区及压力区BV/TV数值差异显著($P < 0.01$,图5A)。在50 g正畸力作用下,大鼠牙槽骨张力区及压力区的多项骨微结构指标随时间发生显著变化。张力区及压力区BV/TV在加力后0~3 d均显著减少($P < 0.001$),压力区3~14 d保持下降趋势,14~28 d持续缓慢回升;而张力区BV/TV在3~7 d缓慢下降后,于14~28 d较快上升至正常水平。Po.V(tot)在3、14、21 d时张力区及压力区差异较大($P < 0.05$,图5B),压力区Po.V(tot)在3~7 d时显著增高,7 d后增量减小,从14 d开始持续下降。张力区Po.V(tot)在0~3 d快速上升,3~7 d增长缓慢,7 d后匀速下降至正常水平。BV/TV和Po.V(tot)增量趋势显示,张力区及压力区数值变化高峰期分别出现在第3天和第7天前,张力区转折点均早于压力区(图6A、B),且3~7 d、14~21 d期间张力区及压力区BV/TV增量差异显著(P 均 < 0.01)。

SMI可反映骨小梁组成中板状和杆状结构的比例,若骨小梁主要为杆状结构,则SMI接近于3。在7、14、21、28 d时两区域SMI差异显著($P < 0.05$,图5C)。压力区SMI在0~3 d、3~7 d快速增加,之后缓慢降低。张力区SMI在0~3 d与压力区数值变化趋势相似,但更早转折,于7 d前后由增到减,21~28 d明显下降。3~7 d期间张力区及压力区SMI增量差异显著($P < 0.01$,图6C)。

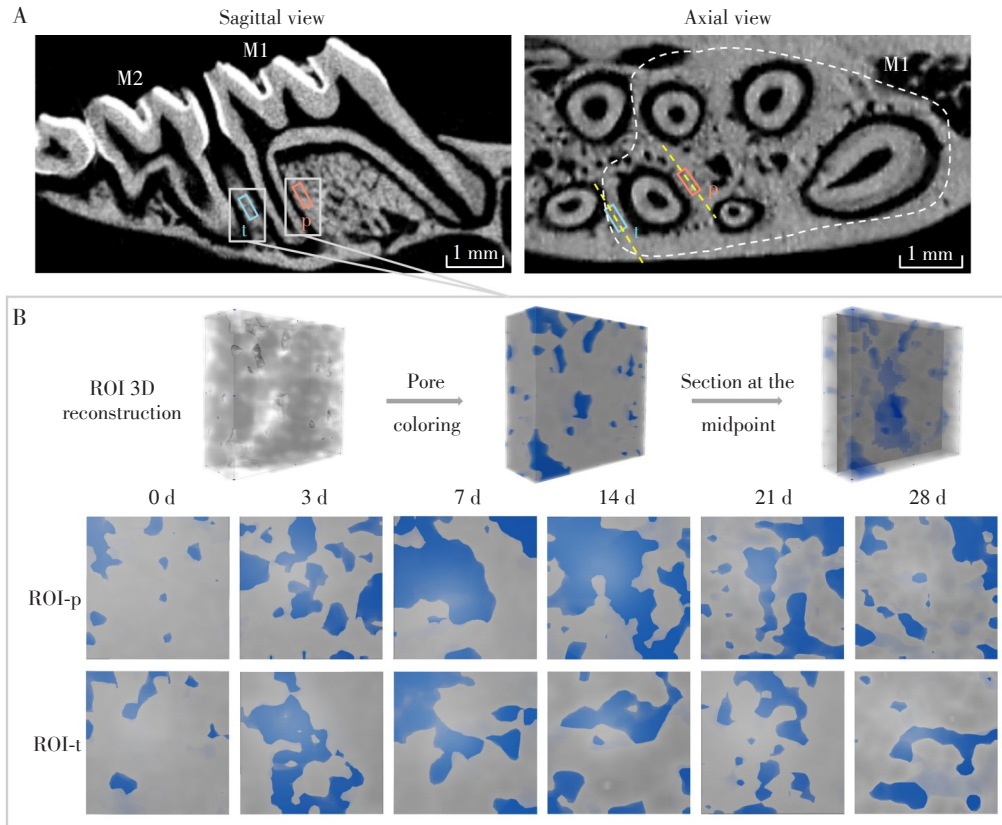
Tb.Th和Tb.Sp在张力区及压力区的变化趋势



A: Sagittal and axial views of 3D reconstruction of orthodontic tooth movement at various time points (scale bar=1 mm). B: Linear fit curve of density-CT value relationship. C: Schematic diagram of centroid distance measurement: M1 represents the first molar, M2 represents the second molar, C1 is the centroid of the first molar, C2 is the centroid of the second molar, and vector \vec{D} is the directed line segment from C2 to C1. D: Trend of tooth movement distance change, $***P < 0.001 (n=5)$.

图3 牙齿移动距离的变化趋势

Figure 3 Trends in orthodontic tooth movement



A: Sagittal and axial CT sections. ROI-p represents the pressure zone, ROI-t represents the tension zone, M1 is the first molar, and M2 is the second molar (scale bar=1 mm). B: 3D reconstruction of ROIs in tension and pressure zones. Blue regions indicate pore areas, while gray regions indicate bone tissue areas.

图4 ROI三维重建截面图

Figure 4 3D reconstructed cross-sectional image of ROI

相似, 分别以7、14 d为转折点。Tb.Th先减后增, 且14~21 d上升趋势最明显; 而Tb.Sp反之(图5D、E)。张力区及压力区Tb.N在7、14、21 d差异有统计学意义($P < 0.05$), 但相同区域内Tb.N随时间无明显变化(图5F)。Tb.Th与Tb.Sp的张力区趋势转折点均早于压力区, 且在7~14 d期间增量差异显著($P < 0.01$, 图6D、E), Tb.N增量正负值持续上下浮动, 无明显变化趋势(图6F)。

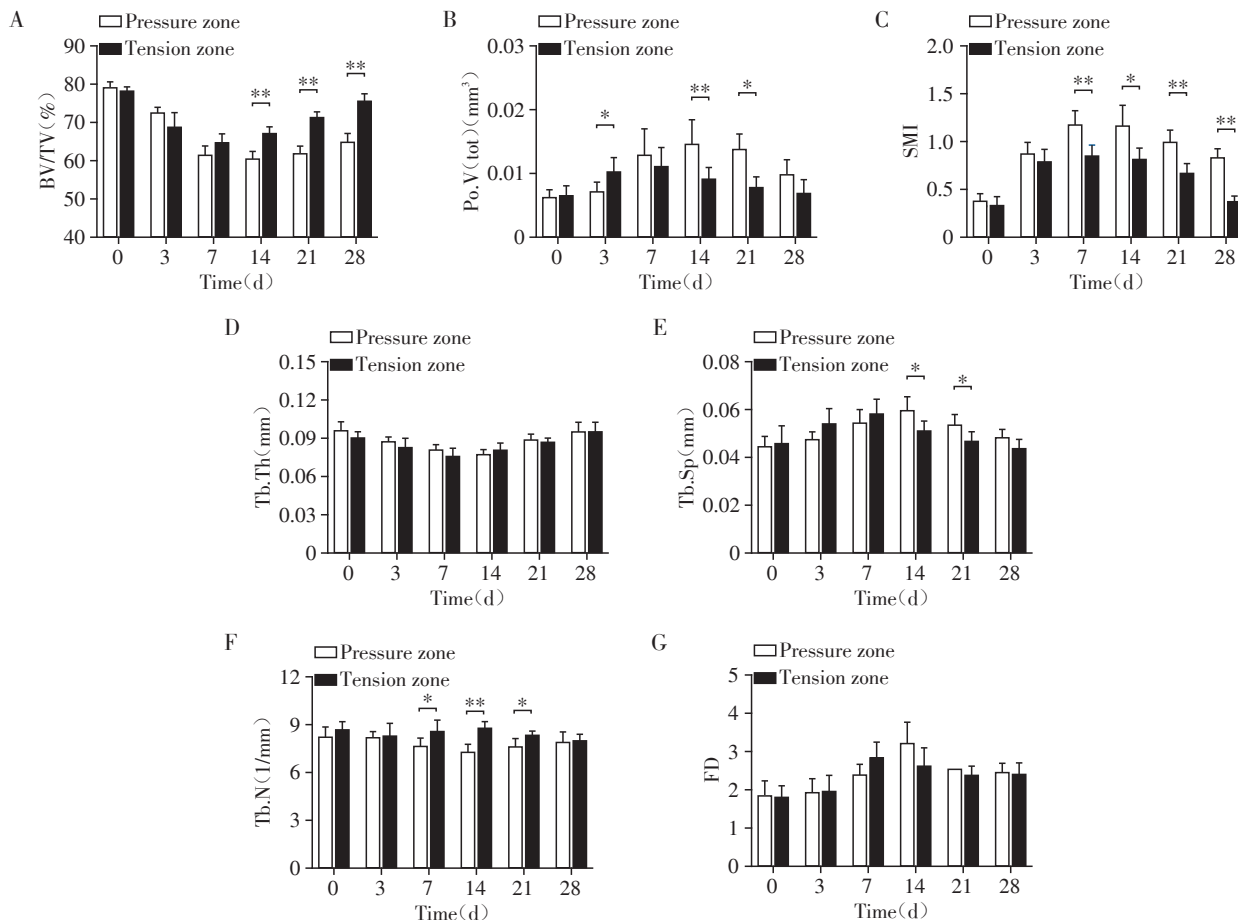
FD适用于描述骨小梁的复杂性及不规则性, 松质骨微结构越复杂, 抗压性越差, 对应的FD值也越大。两区域的FD值变化趋势均为先上升后下降, 张力区及压力区分别在3~7 d与7~14 d时显著增长(图5G), 而后逐渐下降。在7~14 d期间, 两区域的FD增量差异显著($P < 0.05$, 图6G)。

3 讨论

本研究采用Micro-CT活体扫描方案, 对正畸牙

移动大鼠模型开展个体追踪, 构建基于骨性标志点的空间坐标系, 提出新的测量牙移动距离的方法, 并观测和量化正畸力下大鼠张力区及压力区骨小梁微观结构随时间变化的改建趋势及差异。在以往张力区牙槽骨改建情况的研究中, Jiang等^[20]发现张力区骨小梁厚度和BV/TV等参数在加力后前7 d减低, 14 d回升, Wang等^[21]则认为28 d内张力侧骨体积持续下降。此外, 两区域骨微结构变化的差异也存在争议, 有研究显示张力侧多项骨小梁参数在0、3、7 d并无显著变化, 而压力侧骨体积下降^[16, 22], 另有研究指出张力区前14 d骨量和Tb.Th减小幅度较压力区更大^[15]。这些差异一方面可能源于缺乏个体追踪研究, 不同样本骨质的差异性引入误差; 另一方面可能由于张力、压力侧ROI选取方法的不同。

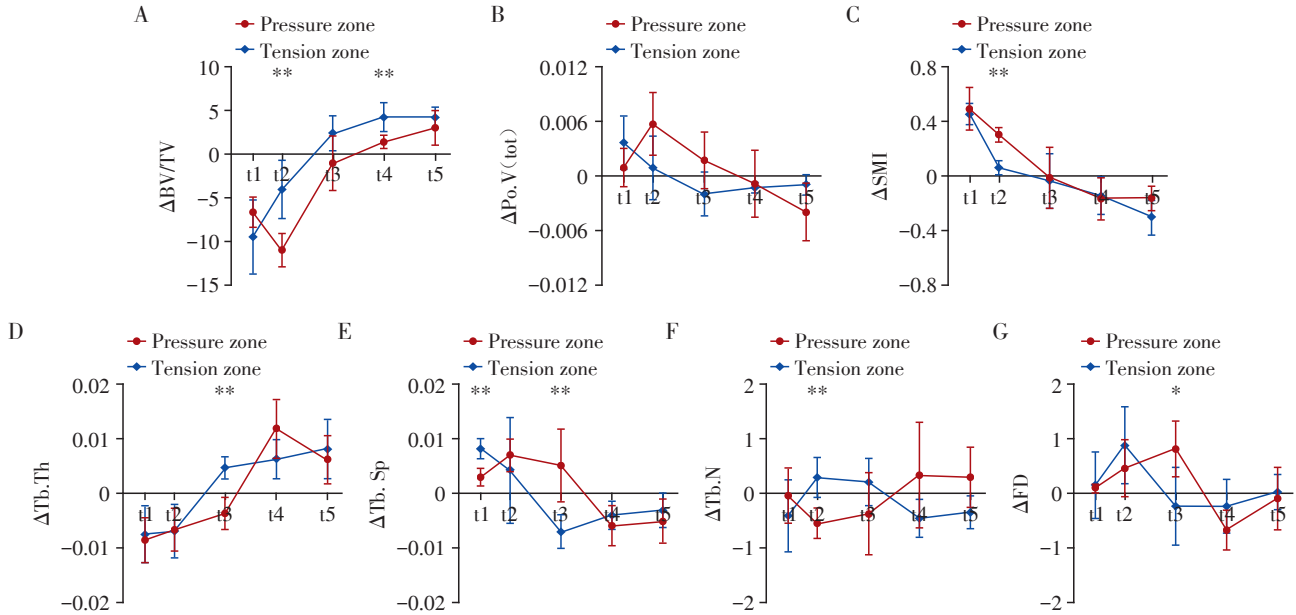
在大鼠第一磨牙的不同牙根中, 近中根体积最大, 有学者以近中根为基准选取ROI^[16, 22], 但该牙根距离施力点较远, 根周应力分布更易受牙齿形态差



A: BV/TV in tension and pressure zones. B: Po.V(tot) in tension and pressure zones. C: SMI in tension and pressure zones. D: Tb.Th in tension and pressure zones. E: Tb.Sp in tension and pressure zones. F: Tb.N in tension and pressure zones. G: FD in tension and pressure zones. * $P < 0.05$ and ** $P < 0.01$ ($n=5$).

图5 张力区及压力区骨小梁形态参数的比较

Figure 5 Comparison of trabecular parameters in tension and pressure zones



A: $\Delta BV/TV$ in tension and pressure zones. B: $\Delta Po.V (tot)$ in tension and pressure zones. C: ΔSMI in tension and pressure zones. D: $\Delta Tb.Th$ in tension and pressure zones. E: $\Delta Tb.Sp$ in tension and pressure zones. F: $\Delta Tb.N$ in tension and pressure zones. G: ΔFD in tension and pressure zones. * $P < 0.05$ and ** $P < 0.01$ ($n=5$). t1=3 d-0 d; t2=7 d-3 d; t3=14 d-7 d; t4=21 d-14 d; t5=28 d-21 d.

图6 张力区及压力区骨小梁参数增量的变化趋势

Figure 6 Trends in the increment of trabecular parameters in tension and pressure zones

异的影响^[23],且近中侧骨质较薄,ROI易靠近皮质骨区域,导致骨量及骨密度等参数测量值偏高^[18]。同时,基于已有的三维有限元研究,正畸力下远中颊根处应力分布最为集中^[17],骨改建效应明显;大鼠第一磨牙的形态差异导致牙齿的旋转中心不完全相同,对其远颊根而言,旋转中心大致处于其根尖区水平^[17],意味着远颊根根尖区以上部位即为高应力集中区^[23]。因此,本研究选择第一磨牙的远中颊根近、远中根中部牙槽松质骨作为ROI,且设置为冠状向截面呈150 $\mu m \times 400 \mu m$ 的长方形,以减少倾斜移动及牙根间距小对受力后骨性质的影响。

本研究活体扫描结果显示,张力区和压力区在骨改建时间点上存在显著差异。压力区的骨吸收活动在加力后3~7 d内最为活跃,表现为骨量显著减少($P < 0.001$)。Li等^[24]发现加力7 d压力侧破骨细胞活跃,验证了这一结论。而张力区的骨吸收在加力后前3 d即开始增加,已有研究发现加力后前3 d张力区破骨细胞数量持续增加^[25],与本研究结果相对应,这表明张力和压力均可诱导破骨细胞分化。增量趋势图显示,张力区及压力区参数转折点分别在7、14 d前后,28 d基本恢复。ROI三维重建显示,张力区的骨量及骨质量先降后升。结合Liu等^[2]和Chen等^[26]的结论,加力后1周成骨细胞表达上调,促进牙移动后期骨生成,提示张力区牙槽骨骨形成滞

后于压力区骨吸收。为确保牙周组织健康,正畸加力需维持一定周期。在骨改建速度方面,张力区及压力区在加力3~7 d BV/TV、SMI和Tb.N增量差异显著,骨吸收阶段张力区改建速度明显快于压力区。这种差异可能与压力侧牙周膜血液灌注受阻有关^[27],引发适应性反应,导致压力区的骨吸收活跃期延迟。此外,参与细胞机械应力信号转导的I型胶原在张力区的比例较高^[28-29],并在牵张力下持续增多^[30],可能促进了张力区的骨改建活动。

松质骨的多孔结构具有非光滑、非规则的特性,但传统评价指标如BV/TV、骨小梁间隙和厚度等^[10-11],难以将骨小梁形态特征与力学属性相关联。有研究表明,骨机械性能与FD密切相关^[31],但量化正畸力下骨小梁复杂度变化的研究较少。本研究通过追踪张力区及压力区FD的变化情况,以评估多孔介质的稳定性。结果显示,加力后7 d两区FD均升至峰值后下降,表明根周骨小梁在骨吸收活跃期排列杂乱、形态差异大,松质骨强度和抗压性降低。可能的解释是骨吸收导致骨小梁表面非均匀凹陷,使骨微结构更加复杂紊乱,FD值上升。

在评估OTM距离时,以往研究多测量第一磨牙远中至第二磨牙近中的间隙^[32],近年来也有学者为减小二维测量误差,利用磨牙三维重建形态拟合平面测距^[21],但以上研究一方面未考虑大鼠磨牙的倾

斜移动,使测量误差普遍存在;另一方面受限于非连续样本,无法构建统一坐标系以准确测量空间参数。因此,本研究基于质心的位移不受牙齿移动类型影响的优势^[33],提出了牙移动距离测量的新方法,以稳定的骨性标志点为基准创建空间坐标系,用第一、第二磨牙质心连线在加力方向上的投影测距,可有效避免因牙齿倾斜移动和扫描平面选取不当而产生的误差。结果显示,牙齿移动分初始快速期(0~3 d)、平台期(3~14 d)和快速线性移动期(14~28 d),这与其他研究报道的3~14 d大鼠牙齿移动速度增加、14~28 d明显下降不一致^[21],原因可能是动物模型的加载力值不同。本研究正畸牙齿移动呈阶段性,与经典研究相符^[34],结合Baxter等^[35]的研究结果推测,大鼠牙移动早期因牙周膜缺血引起的透明样变而受阻,随后牙周膜动态再生,因此牙齿移动速率并非保持一致。关于多次扫描后Micro-CT辐射对大鼠牙槽骨改建的影响,Mustafy等^[36]证明在0.83 Gy辐射剂量下每周1次活体扫描不会影响大鼠的骨骼质量和骨微观结构,但不同扫描方案对牙齿移动的影响仍需更多研究明确。

综上所述,本研究针对以往研究所存在的共性问题,提出了新的实验方案及牙移动测量方法,建立统一坐标系精确测量空间参数,对于形态参数,可获取随时间变化的动态数据,为OTM机制研究提供参考。研究结果显示大鼠OTM具有三阶段特征,张力区及压力区骨量及骨质量均先下降后上升,且分别在7 d和14 d时抗压性最弱。此外,张力区较压力区更早进入骨吸收活跃期,而张力侧牙槽骨骨形成滞后于压力侧骨吸收。这些结论提示,正畸力施加初期,临床应关注张力区的骨改建情况,同时避免压力区应力过大引发异常骨吸收,必要时可根据不同患者的骨质状况制定个性化的矫治方案。最后,本研究样本较局限,尚停留在形态学分析,未来研究应增加样本量并考虑年龄及性别因素,还需从分子生物学角度进一步探索牙槽骨改建的生物学和力学机制,完善对OTM机制的理解。

利益冲突声明:

所有作者声明无利益冲突。

Conflict of Interests:

The authors declared no conflict of interests.

作者贡献声明:

钱心瑶负责研究设计,实施实验,数据收集与分析,文章撰写;姜迪负责研究设计,数据分析,文章审阅和修改;谢玉婷负责数据分析,公式推导;吴斌负责研究设计,文章审阅;唐雯、陆玲波、李禹江协助实验,参与文章校对修订;严斌、谢

理哲负责研究设计与实验指导,论文审阅。

Author's Contributions:

QIAN Xinyao was responsible for research design, implementation of experiments, data collection and analysis, and manuscript writing; JIANG Di was responsible for research design, data analysis, manuscript review and revision; XIE Yuting was responsible for data analysis and formula derivation; WU Bin was responsible for research design and manuscript review; TANG Wen, LU Lingbo, and LI Yujiang assisted in experiments, proofreading and revising the manuscript; YAN Bin and XIE Lizhe were responsible for research design, experimental guidance, and manuscript review.

[参考文献]

- [1] LIN J Y, HUANG J C, ZHANG Z Q, et al. Periodontal ligament cells under mechanical force regulate local immune homeostasis by modulating Th17/Treg cell differentiation [J]. Clin Oral Investig, 2022, 26(4): 3747-3764
- [2] LIU Y B, AI Y L, SUN X, et al. Interleukin-20 acts as a promotor of osteoclastogenesis and orthodontic tooth movement [J]. Stem Cells Int, 2021, 2021: 5539962
- [3] LIMA F, DEFALCO V, BAIMA J, et al. Effect of impact load and active load on bone metabolism and body composition of adolescent athletes [J]. Med Sci Sports Exerc, 2001, 33(8): 1318-1323
- [4] RUIJERMAN R, VAN-RIETBERGEN B, HILBERS P, et al. The effects of trabecular-bone loading variables on the surface signaling potential for bone remodeling and adaptation [J]. Ann Biomed Eng, 2005, 33(1): 71-78
- [5] ZHUANG L, BAI Y X, MENG X Y. Three-dimensional morphology of root and alveolar trabecular bone during tooth movement using micro-computed tomography [J]. Angle Orthod, 2011, 81(3): 420-425
- [6] MILNE T J, ICHIM I, PATEL B, et al. Induction of osteopenia during experimental tooth movement in the rat: alveolar bone remodelling and the mechanostat theory [J]. Eur J Orthod, 2009, 31(3): 221-231
- [7] HSU J T, CHANG H W, HUANG H L, et al. Bone density changes around teeth during orthodontic treatment [J]. Clin Oral Investig, 2011, 15(4): 511-519
- [8] WAGNER D, EL-HAFICI H, BENSIDHOUM M, et al. Periodontal ligament histology for orthodontic bone remodeling: first quantification [J]. J Cell Immunother, 2018, 4(1): 41-43
- [9] MENA-LAURA E E, CESTARI T M, ALMEIDA R, et al. Metformin as an add-on to insulin improves periodontal response during orthodontic tooth movement in type 1 diabetic rats [J]. J Periodontol, 2019, 90(8): 920-931
- [10] KRAIWATTANAPONG K, SAMRUJAJENJAKUN B.

- Effects of different force magnitudes on corticotomy-assisted orthodontic tooth movement in rats[J]. *Angle Orthod*, 2018, 88(5): 632-637
- [11] JINDAROJANAKUL C, SAMRUAJBENJAKUN B. Influence of ibuprofen combined with corticotomy on tooth movement and alveolar bone remodeling in rats[J]. *Angle Orthod*, 2022, 92(6): 773-779
- [12] AN J T, LI Y, LIU Z S, et al. A micro-CT study of micro-structure change of alveolar bone during orthodontic tooth movement under different force magnitudes in rats [J]. *Exp Ther Med*, 2017, 13(5): 1793-1798
- [13] 陈 鹏, 杨风雪, 周建萍, 等. Micro-CT动态观察大鼠牙齿移动过程中微观结构的变化[J]. *上海交通大学学报(医学版)*, 2017, 37(2): 193-198
- CHEN P, YANG F X, ZHOU J P, et al. Micro-structure changes in rat tooth movement process through micro-computed tomography dynamic observation[J]. *Journal of Shanghai Jiaotong University(Medical Science)*, 2017, 37(2): 193-198
- [14] 庄 丽, 孟宪莹, 白玉兴. 正畸牙齿移动过程中牙槽骨的Micro-CT形态学研究[J]. *北京口腔医学*, 2009, 17(4): 181-183
- ZHUANG L, MENG X Y, BAI Y X. Morphological changes of alveolar bone during orthodontic tooth movement on Micro-CT[J]. *Beijing Journal of Stomatology*, 2009, 17(4): 181-183
- [15] XU B W, YANG K. Changes in alveolar bone structure during orthodontic tooth movement in adolescent and adult rats: a microcomputed tomography study[J]. *Orthod Craniofac Res*, 2023, 26(4): 568-575
- [16] RU N, LIU S S, ZHUANG L, et al. *In vivo* microcomputed tomography evaluation of rat alveolar bone and root resorption during orthodontic tooth movement[J]. *Angle Orthod*, 2013, 83(3): 402-409
- [17] GONZALES C, HOTOKEZAKA H, ARAI Y, et al. An *in vivo* 3D micro-CT evaluation of tooth movement after the application of different force magnitudes in rat molar[J]. *Angle Orthod*, 2009, 79(4): 703-714
- [18] 魏占英, 章振林. Micro-CT在骨代谢研究中骨微结构指标的解读及应用价值[J]. *中华骨质疏松和骨矿盐疾病杂志*, 2018, 11(2): 200-205
- WEI Z Y, ZHANG L. Interpretation and application of Micro-CT to obtain microstructure index in bone metabolism research [J]. *Chinese Journal of Osteoporosis and Bone Mineral Research*, 2018, 11(2): 200-205
- [19] CLARK D P, BADEA C T. Advances in micro-CT imaging of small animals[J]. *Phys Med*, 2021, 88: 175-192
- [20] JIANG Y K, TAO G Y, GUAN Y Z, et al. The role of ephrinB2-EphB4 signalling in bone remodelling during orthodontic tooth movement[J]. *Orthod Craniofac Res*, 2023, 26(1): 107-116
- [21] WANG C, CAO L, YANG C S, et al. A novel method to quantify longitudinal orthodontic bone changes with *in vivo* micro-CT data[J]. *J Healthc Eng*, 2018, 2018: 1651097
- [22] 茹 楠, 庄 丽, 白玉兴. 牙齿移动过程中牙槽骨显微结构动态变化的微型CT研究[J]. *中华口腔医学杂志*, 2011, 46(4): 237-240
- RU N, ZHUANG L, BAI Y X. Evaluation of periodontal tissue during orthodontic tooth movement in rats: a micro-computed [J]. *Chinese Journal of Stomatology*, 2011, 46(4): 237-240
- [23] JAIN A, PRASANTHA G S, MATHEW S, et al. Analysis of stress in periodontium associated with orthodontic tooth movement: a three dimensional finite element analysis[J]. *Comput Methods Biomech Biomed Engin*, 2021, 24(16): 1841-1853
- [24] LI X, LI M, LU J, et al. Age-related effects on osteoclastic activities after orthodontic tooth movement[J]. *Bone Joint Res*, 2016, 5(10): 492-499
- [25] YOSHIDA T, YAMAGUCHI M, UTSUNOMIYA T, et al. Low-energy laser irradiation accelerates the velocity of tooth movement *via* stimulation of the alveolar bone remodeling[J]. *Orthod Craniofac Res*, 2009, 12(4): 289-298
- [26] CHEN S, HUANG D Y, ZHU L, et al. Contribution of diabetes mellitus to periodontal inflammation during orthodontic tooth movement[J]. *Oral Dis*, 2024, 30(2): 650-659
- [27] LORIER G, TOURIÑO C, KALIL R A K. Coronary angiogenesis as an endogenous response to myocardial ischemia in adults[J]. *Arq Bras Cardiol*, 2011, 97(6): 140-148
- [28] XU H, HAN X L, MENG Y, et al. Favorable effect of myofibroblasts on collagen synthesis and osteocalcin production in the periodontal ligament[J]. *Am J Orthod Dentofacial Orthop*, 2014, 145(4): 469-479
- [29] ABUHASHISH H, ALAMRI A, SHAHIN S, et al. Bevacizumab, a vascular endothelial growth factor inhibitor, promotes orthodontic tooth movement in an experimental rat model[J]. *Heliyon*, 2023, 9(5): e16217
- [30] SIADAT S M, RUBERTI J W. Mechanochemistry of collagen[J]. *Acta Biomater*, 2023, 163: 50-62
- [31] GARCÍA - VILANA S, SÁNCHEZ - MOLINA D, VELÁZQUEZ-AMEIJIDE J, et al. Relation between mechanical and densitometric properties to fractal dimension in human rib cortical bone[J]. *Med Eng Phys*, 2023, 117: 104004
- [32] FLEISSIG O, HAZAN-MOLINA H, CHAUSHU S, et al.

- microbial lipopeptides in human macrophages[J]. *Immunity*, 2012, 36(3):464-476
- [23] WANG K, TIAN J, ZHENG C, et al. Interpretable prediction of 3-year all-cause mortality in patients with heart failure caused by coronary heart disease based on machine learning and SHAP[J]. *Comput Biol Med*, 2021, 137: 104813
- [24] BURCHALL G, LINDEN M D, TEEDE H, et al. Hemostatic abnormalities and relationships to metabolic and hormonal status in polycystic ovarian syndrome [J]. *Trends Cardiovasc Med*, 2011, 21(1):6-14
- [25] LI Y, CHEN C Y, MA Y, et al. Multi-system reproductive metabolic disorder: significance for the pathogenesis and therapy of polycystic ovary syndrome (PCOS) [J]. *Life Sci*, 2019, 228: 167-175
- [26] SADEGHI A, FADAEI R, MORADI N, et al. Circulating levels of C1q/TNF- α -related protein 6 (CTRP6) in polycystic ovary syndrome [J]. *IUBMB Life*, 2020, 72(7): 1449-1459
- [27] AZUMAH R, LIU M H, HUMMITZSCH K, et al. Candidate genes for polycystic ovary syndrome are regulated by TGF β in the bovine foetal ovary [J]. *Hum Reprod*, 2022, 37(6):1244-1254
- [28] RUDNICKA E, SUCHTA K, GRYMOWICZ M, et al. Chronic low grade inflammation in pathogenesis of PCOS [J]. *Int J Mol Sci*, 2021, 22(7): 3789
- [29] OH S, LEE J, OH J, et al. Integrated NLRP3, AIM2, NLRC4, Pyrin inflammasome activation and assembly drive PANoptosis [J]. *Cell Mol Immunol*, 2023, 20(12): 1513-1526
- [30] ROSTAMTABAR M, ESMAEILZADEH S, KARKHAH A, et al. Elevated expression of IL-18 but not IL-1 β gene is associated with NALP3 and AIM2 inflammasome in polycystic ovary syndrome [J]. *Gene*, 2020, 731: 144352
- [31] LI C, LIU Q, XIE L Q. Suppressing NLRP2 expression accelerates hepatic steatosis: a mechanism involving inflammation and oxidative stress [J]. *Biochem Biophys Res Commun*, 2018, 507(1/2/3/4):22-29
- [32] STIENSTRA R, VAN-DIEPEN J A, TACK C J, et al. Inflammasome is a central player in the induction of obesity and insulin resistance [J]. *Proc Natl Acad Sci U S A*, 2011, 108(37): 15324-15329
- [收稿日期] 2024-09-29
(本文编辑: 陈汐敏)

(上接第486页)

- Analytical methodology to measure periodontal bone morphometry following orthodontic tooth movement in mice [J]. *Eur J Orthod*, 2021, 43(6): 665-671
- [33] KONDO T, HOTOKEZAKA H, HAMANAKA R, et al. Types of tooth movement, bodily or tipping, do not affect the displacement of the tooth's center of resistance but do affect the alveolar bone resorption [J]. *Angle Orthod*, 2017, 87(4): 563-569
- [34] SMITH R J, BURSTONE C J. Mechanics of tooth movement [J]. *Am J Orthod*, 1984, 85(4): 294-307
- [35] BAXTER S J, SYDORAK I, MA P X, et al. Impact of pharmacologic inhibition of tooth movement on periodontal and tooth root tissues during orthodontic force application [J]. *Orthod Craniofac Res*, 2020, 23(1): 35-43
- [36] MUSTAFY T, BENOIT A, LONDONO I, et al. Can repeated *in vivo* micro-CT irradiation during adolescence alter bone microstructure, histomorphometry and longitudinal growth in a rodent model? [J]. *PLoS One*, 2018, 13(11): e0207323
- [收稿日期] 2024-11-18
(本文编辑: 陈汐敏)